Renewable Energy 219 (2023) 119520

Contents lists available at ScienceDirect

Renewable Energy

journal homepage: www.elsevier.com/locate/renene

# Experimental investigation of a co-located wind and wave energy system in regular waves

Eric Gubesch [b], Nataliia Y. Sergiienko [a,*], Jean-Roch Nader [b], Boyin Ding [a], Benjamin Cazzolato [a], Irene Penesis [d,b], Ye Li [c]

[a] The University of Adelaide, School of Electrical and Mechanical Engineering, Adelaide, 5005, SA, Australia
[b] Australian Maritime College, University of Tasmania, Launceston, 7250, TAS, Australia
[c] Multiple Function Towing Tank Laboratory, Shanghai Jiao Tong University, Shanghai, 200240, China
[d] Blue Economy Cooperative Research Centre, Launceston, 7250, TAS, Australia

ARTICLE INFO

*Keywords:*
Co-located offshore wind and wave energy converter
Wind turbine
Wave energy converter
Combined wind-wave
Load reduction
Physical experiments

ABSTRACT

The integration of wave energy converters (WECs) into offshore wind farms offers a promising solution to potentially reduce the cost of both technologies. In a co-located wind-wave system, in addition to generating electricity, WECs can be used to reduce wave forces acting on the support structure of a wind turbine. This work aims to investigate the interactions between a fixed-bottom wind turbine substructure and a heaving WEC with a primary focus on wind turbine wave loads. For this purpose, physical experiments are developed and carried out using a 1:13 scale model of the WEC and the support structure of a wind turbine (monopile) in regular waves. The results demonstrate that active control of WEC motion can lead to a significant reduction in the horizontal forces acting on the wind turbine substructure.

## 1. Introduction

Wind energy is a leading renewable technology, accounting for over 6% of global electricity production [1]. It is expected that wind energy will become one of the dominant energy sources in the future, and offshore wind is an essential pillar of this transition [2]. Over the past 10 years, offshore wind has matured and is by far the most advanced offshore renewable technology [3]. On the other hand, the wave energy industry is developing slowly. This is largely due to economic challenges associated with developing competitive technology that reduces the levelised cost of electricity (LCOE) [4]. There is an opportunity to develop a mutually beneficial relationship between the growing offshore wind energy industry and wave energy technology developers.

Currently, the vast majority of offshore wind farms have fixed-bottom foundations suitable for water depths of up to 40–60 m [5]. Within various design ideas, the monopile is considered to be the most robust foundation concept for offshore wind [6], and it makes up approximately 70% of all installations [5]. The structural integrity of the monopile foundation and tower is directly affected by the dynamic loading arising from turbulent wind, ocean waves, and rotor excitation. As a result, capital and operational expenditures may increase leading to elevated LCOE [7–10]. Therefore, reducing the load on the support structure has the potential to reduce the energy cost of offshore wind, making the technology more economically competitive in the long term.

A potential solution for reducing wave loading on wind turbine substructure is associated with the use of co-located wave energy converters (WECs) [11,12]. WECs operate by converting hydrodynamic energy from the incident waves into kinetic energy via rigid body motions (e.g., heave). The kinetic energy is then converted into electricity via a power take-off (PTO) system. The WEC's motions may be tuned with a reactive control system to optimise power absorption [13]. During this process, the WEC's motions affect the incident wavefield via diffraction and radiation. These wavefield interactions are directly related to the WEC's submerged geometry and the relative amplitude and phase of its motions. Therefore, installing WECs upstream from the offshore wind farm might create a shadow effect that protects the wind farm from harmful wave loading [14] and increase the weather window for operation and maintenance (O&M) activities. Additionally, co-located offshore wind and WEC's may allow electrical infrastructure to be shared (offshore substations and subsea transmission cables), which may help reduce substantial economic barriers to the wider wave energy industry. Supplementary benefits include the smoothed power output from two sources of renewable energy, common logistics and O&M, potential cost reduction [15] and enhanced economic viability for both wind turbines and wave energy [16,17].

* Corresponding author.
*E-mail address:* nataliia.sergiienko@adelaide.edu.au (N.Y. Sergiienko).

https://doi.org/10.1016/j.renene.2023.119520
Received 29 December 2022; Received in revised form 18 October 2023; Accepted 24 October 2023
Available online 27 October 2023
0960-1481/© 2023 The Author(s). Published by Elsevier Ltd. This is an open access article under the CC BY license (http://creativecommons.org/licenses/by/4.0/).

Various configurations for combined wave and wind systems have been recommended and investigated. Pérez-Collazo et al. [15] provided a comprehensive review of combined wind-wave systems which can be categorised into co-located, hybrid, or island systems. Co-located wind-wave systems combine independent offshore wind turbines and WECs. Here, the wind turbines and WEC's do not share foundations or structural components, however, may share electrical and operational infrastructure. Hybrid wind-wave systems integrate a WEC and wind turbine into a single fixed or floating structure. Island systems are an extension of hybrid systems, where multiple WECs and wind turbines are combined into a much larger structure. Pérez-Collazo et al. [15] state that a large volume of research and development has been devoted to hybrid wind-wave systems in recent years, however, suggests that co-located systems are likely to be a *'first approach'* due to lower risk profiles and reduced development costs.

Considering hybrid WEC and fixed-bottom wind turbines, the combination of an oscillating water column (OWC) and a jacket-frame support substructure has been proposed in [18]. Following this, the OWC has been attached to a monopile substructure and presented in [19]. The performance of both hybrid wind-wave systems has been evaluated with physical experiments in a wave basin with attention given to the WEC power production and changes in the wave field due to the presence of the WEC. The potential of combining a heaving torus-type WEC with a monopile has been examined in [20] primarily focusing on the WEC power output. Jiang et al. [21] have investigated the structural energy transfer between a hybrid jacket foundation and a wind-wave coupling device. Many studies have also investigated floating hybrid wind-wave systems. For example, Fenu et al. [22] have used a physical experiment to examine the response of a hybrid multi-OWC and wind turbine system that was integrated into a deep draught floater (i.e., spar). In this case, three OWCs have been attached to the substructure of the floating wind turbine. Similarly, da Silva et al. [12] and Zhou et al. [23] have investigated multiple heaving point absorbers connected to a floating semi-submersible offshore wind turbine.

A good example of an island wind-wave system is the P37 and P80 prototype [24–26]. This platform has been tested at sea for a two-year period off the Denmark coast. The hybrid system incorporated three wind turbines and ten oscillating water column WECs onto a floating semi-submersible structure. Numerous physical experiments and numerical simulations have been conducted in the year prior to deployment [25]. Yde et al. [26] have compared numerical results to offshore measurement data of the deployed P37 prototype and found that the numerical model (in this case, HAWC2–WAMIT) could capture platform motion to some extent. The article concludes by acknowledging *"One of the key challenges in the development of combined wind and wave energy devices is the development of reliable numerical models to predict the loads and motions on the devices under different sea and wind conditions"*. This implies that wind-wave coupled systems display challenging hydrodynamic responses and may require significant understanding to interpret and predict behaviour accurately with numerical simulations.

Considering co-located wind-wave farms, various research has investigated selecting optimum locations for co-located wave and wind energy farms [27,28], economic modelling [29,30], energy production [31], and optimal geometric arrangements for improved power production and reductions in incident wave height [32,33]. However, despite these important considerations, very few studies have examined the specific interactions between co-located WECs and offshore wind turbines, relating directly to environmental loading and structural integrity. Clark et al. [34] have studied fatigue loading of wind turbine monopile foundations in co-located wind-wave farms. Findings from Clark et al. [34] indicate that a single WEC can reduce monopile fatigue loads by 8%, whereas an array of WECs can reduce fatigue loads by 10%. Gubesch et al. [35] experimentally investigated the interactions between a co-located heaving WEC and wind turbine substructure. This study evaluated how the amplitude and phase of a heaving point absorber affected the wave loads on a fixed offshore wind turbine substructure. Findings from [35] showed that the WEC's motions (i.e., amplitude and phase) can have a significant effect on the wind turbine wave loading.

The power generated by the WEC is clearly one of the key criteria when evaluating the feasibility of the wind-wave system. However, less consideration has been given to the use of co-located WECs to reduce the wave load on a wind turbine substructure. Therefore, the main aim of this study is to evaluate if the forces acting on an offshore wind turbine can be reduced by controlling the motion of a heaving WEC, and if so, how does this affect the harvested wave power. To address this gap in knowledge, a comprehensive set of physical experiments and numerical modelling was used to evaluate and investigate the interactions between a co-located heaving WEC and a fixed offshore wind turbine substructure. The WEC and wind turbine in this study do not share foundations or structural components, however, are positioned in close proximity to each other.

This study investigates the hydrodynamic responses when the co-located wind-wave systems are subjected to small amplitude regular waves. Considering that Yde et al. [26] expressed difficulty when numerically modelling the hydrodynamic responses with the P37, small amplitude waves are selected to understand the fundamental interactions between the WEC's motions and wave loading on the wind turbine substructure before introducing the complexity and uncertainty associated with the nonlinearities in extreme irregular waves (i.e., survivable conditions). A complementary numerical analysis is used throughout the paper, not for verification purposes but to build a deeper understanding of the investigated problem. The experimental and numerical techniques chosen for use in this study are designed to accommodate and complement the limitations of each method. For example, the experimental investigation is used to capture the complex wave and structure interactions between the WEC and wind turbine substructure. These include nonlinear interactions and effects from viscosity and turbulence which may not be captured in the numerical model. Additionally, the physical experiments provide an opportunity to record each test with high-resolution, high-speed video footage. On the other hand, the validated numerical models provide an opportunity to investigate hydrodynamic aspects that could not be studied during the physical experiments due to limitations with some electrical components. For example, the use of active control theory for the WEC's motions could not be completed in the experiment due to a lack of a real-time controller. The combination of both physical experiments and numerical modelling provides greater insight into the specific interactions between a heaving WEC and the fixed offshore wind turbine substructure.

The article is structured as follows. Section 2 contains the theoretical background for this study. The experimental setup and equivalent numerical model are explained in Section 3. Experimental results are presented in Section 4 and discussed in Section 5. Limitations of the current study and future work directions are covered in Section 6. Finally, conclusions are drawn in Section 7.

## 2. Phenomenological theory

Consider a system of two bodies that interact with ocean waves: a fixed-bottom wind turbine (monopile) and a floating wave energy converter. When both bodies are fixed and not moving with waves, they only experience the wave excitation force that also includes diffraction effects caused by the presence of other bodies. However, when the WEC starts to oscillate with a particular velocity, it radiates waves that create an additional force on the wind turbine substructure. This additional force depends on the amplitude, phase and frequency of the WEC oscillation, mode of oscillation (surge, heave, or pitch), as well as the geometry of the problem [36]. Using the principle of the superposition,

the total force acting on the wind turbine (WT) substructure can be written in vector form as [37]:

$$\hat{\mathbf{F}}^{\mathrm{WT}}_{\mathrm{tot}} = \hat{\mathbf{F}}^{\mathrm{WT}}_{\mathrm{exc}} - \mathbf{Z}^{\mathrm{WT}}_{\mathrm{WEC}}\hat{\mathbf{u}}^{\mathrm{WEC}}, \tag{1}$$

where $\hat{\mathbf{F}}^{\mathrm{WT}}_{\mathrm{tot}}$ is the total force vector acting on the wind turbine substructure, $\hat{\mathbf{F}}^{\mathrm{WT}}_{\mathrm{exc}}$ is the wind turbine excitation force vector, $\mathbf{Z}^{\mathrm{WT}}_{\mathrm{WEC}}$ is a $6 \times 6$ radiation-impedance matrix that can be decomposed into the radiation damping and added mass matrices $\mathbf{Z}^{\mathrm{WT}}_{\mathrm{WEC}} = \mathrm{i}\omega\mathbf{A}^{\mathrm{WT}}_{\mathrm{WEC}} + \mathbf{B}^{\mathrm{WT}}_{\mathrm{WEC}}$, $\hat{\mathbf{u}}^{\mathrm{WEC}}$ is the vector of the buoy velocities. The $\hat{(}$ symbol represents the complex-amplitude of the harmonic oscillation according to the following convention [38]:

$$x(t) = x_0\cos(\omega t + \varphi_x) = \Re\mathfrak{e}\{x_0 e^{\mathrm{i}(\omega t+\varphi_x)}\} = \Re\mathfrak{e}\{\hat{x}e^{\mathrm{i}\omega t}\}, \tag{2}$$

where $x_0$ is the amplitude, and $\varphi_x$ is the phase.

If the WEC oscillates in heave mode with a complex velocity amplitude of $\hat{u}_z = \mathrm{i}\omega\hat{z}$, the total horizontal force acting on the wind turbine substructure is:

$$\hat{F}^{\mathrm{WT}}_{tot,x} = \hat{F}^{\mathrm{WT}}_{exc,x} - (-\omega^2 A_{1,9} + \mathrm{i}\omega B_{1,9})\hat{z}^{\mathrm{WEC}}, \tag{3}$$

and the total overturning (pitch) moment is:

$$\hat{M}^{\mathrm{WT}}_{tot,y} = \hat{M}^{\mathrm{WT}}_{exc,y} - (-\omega^2 A_{5,9} + \mathrm{i}\omega B_{5,9})\hat{z}^{\mathrm{WEC}}. \tag{4}$$

The indices of matrices **A** and **B** are specified according to the numbering convention used in various numerical hydrodynamic solvers (i.e. NEMOH and WAMIT). For example, assuming that the wind turbine substructure is the body 1, and the WEC is the body 2, and each body has 6 modes, either fixed or free, (surge, sway, heave, roll, pitch and yaw), the index (1,9) corresponds to the first mode of the wind turbine substructure (surge, or horizontal), and the third ($9 - 6 = 3$) mode of the WEC (heave, or vertical).

Eqs. (3) and (4) demonstrate that the wave loading on the wind turbine substructure can be decreased by properly adjusting the amplitude and phase of the WEC motion.

## 3. Experimental and numerical modelling

The combined wind-wave system studied in this paper is illustrated in Fig. 1. The physical experiments have been designed to investigate the loading on the wind turbine support structure (monopile) and dynamics of the combined wind-wave system in shallow-water conditions. For specific details, refer to Gubesch et al. [35]. Both the monopile and the WEC are cylindrical in shape with a constant radius along the wetted surface. The physical experiments have been designed as a theoretical study to evaluate the fundamental interactions between the WEC and wind turbine substructure. The geometry of the wind turbine substructure and target wavefield is designed such that the scatter parameter ($kR$) ranged between 0.6 and 1.25 while not exceeding the maximum capacity of the load cell in extreme waves. This is due to a secondary set of experiments that have been conducted during the same campaign. The dimensions (draft and diameter) of the WEC are chosen to be as large as possible, but limited by the capacity of the linear motor and load cell. The geometry and spacing of the WEC and wind turbine substructure have been investigated numerically before the experiments. Pre-experimental numerical analysis indicated that the WEC should be positioned near the wind turbine substructure to reduce wave loading. The final geometry and spacing have been then normalised for ease of communication to the research community (i.e., the WEC's diameter is $\approx 2/3$ of the wind turbine monopile diameter, and the WEC is positioned one monopile diameter forward of the wind turbine substructure).

As this study has been designed as a theoretical work, there is no specific experimental full-scale equivalent, however, the data can be scaled accordingly with Froude similitude laws. For example, a scale factor of 1:13 would replicate a full-scale monopile diameter of 10 m which is capable of supporting a 15-MW wind turbine [39,40]. The experimental and full-scale parameters of the wind turbine monopile and the WEC are specified in Table 1.

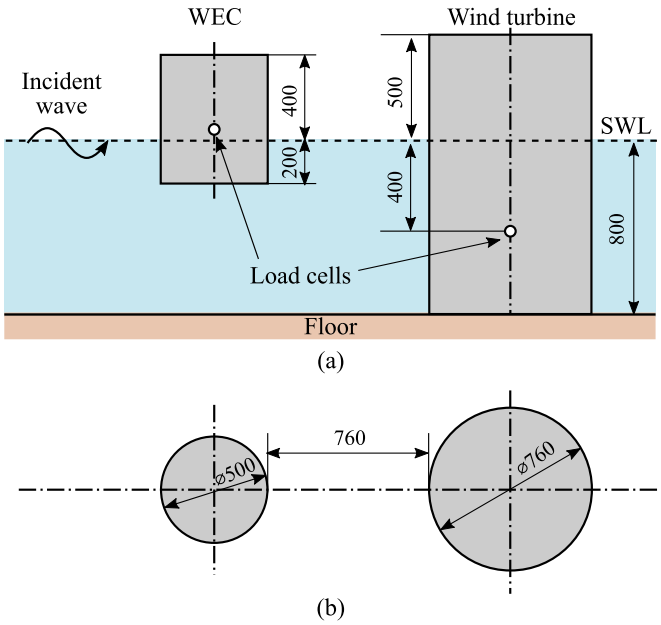


**Fig. 1.** Geometry of the studied combined wind-wave system: (a) side view, (b) top view.

**Table 1**
Parameters of the combined wind-wave system.

| Parameter | Unit | Experimental | Full scale |
|---|---|---|---|
| Wind turbine substructure | | | |
| Diameter ($2a^{\mathrm{WT}}$) | m | 0.76 | 10 |
| Load-cell location (below SWL) | m | 0.4 | 5.26 |
| WEC | | | |
| Diameter ($2a^{\mathrm{WEC}}$) | m | 0.5 | 6.58 |
| Height | m | 0.6 | 7.89 |
| Draft | m | 0.2 | 2.63 |
| Load-cell location (above SWL) | m | 0.0175 | |
| Water depth ($h$) | m | 0.8 | 10.53 |
| Distance between WT and WEC walls | m | 0.76 | 10 |
| Distance between WT and WEC centres ($D$) | m | 1.39 | 18.3 |

Note: SWL refers to the still water level.

### 3.1. Physical experiments

Physical experiments are conducted in the Model Test Basin (MTB) at the Australian Maritime College, University of Tasmania (see Fig. 2). The MTB has a length of 35 m, a width of 12 m and a water depth of 0.8 m. The waves are generated with a HR Wallingford piston-type wavemaker (16 paddles). A 1:6 porous beach is located at the aft end of the MTB which is designed to damp wave reflections. The WEC has a 25 mm fillet around the submerged edge to reduce the turbulence that may be generated in high amplitude, high frequency heave motions. The WEC's heave motions are controlled by a linear actuator (LinMot) which is mounted above the WEC on a rigid overhead structure and measured with a linear variable displacement transducer (LVDT). The forces and moments on the WEC and wind turbine are measured with six degree of freedom (6-DoF) load cells. The incident waves are measured with resistive wave probes.

For reference only, the problem geometry and tested wave conditions with respect to the wavelength are specified in Table 2. The considered ratios of the wind turbine diameter to the wavelength ($2a^{\mathrm{WT}}/\lambda$) are higher than 0.09, meaning that the contribution of the viscous drag forces to the total hydrodynamic force can be neglected [41]. The ratio of the water depth to the wavelength demonstrates that tested conditions include deep ($h/\lambda > 0.5$) and transitional-water waves ($0.05 < h/\lambda < 0.5$). Both wave steepness ($H/\lambda$) and water depth ($h$)

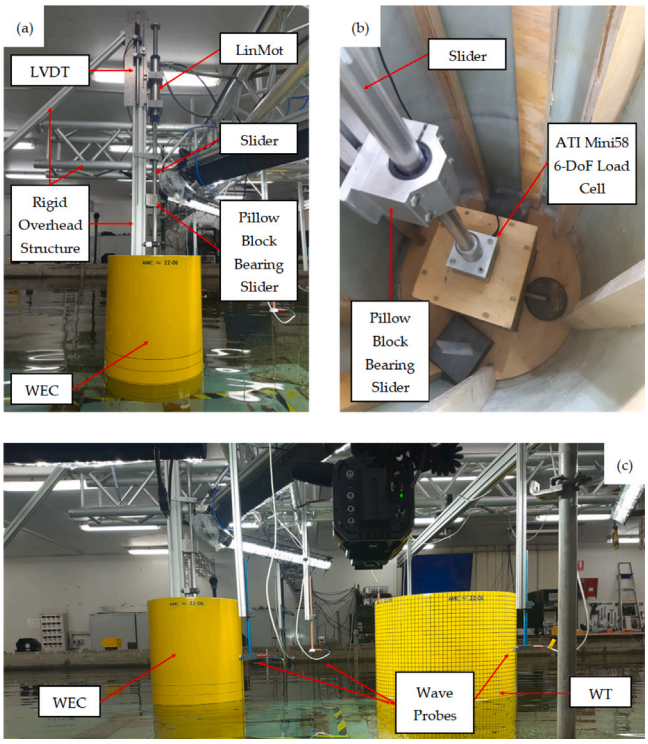


**Fig. 2.** Experimental setup of the combined wind-wave system: (a) heaving WEC attached to linear motor, (b) load cell mounted on WEC, (c) co-located wind turbine and WEC.

**Table 2**
Nondimensional experimental conditions.

| Parameter | From | To |
|---|---|---|
| WT diameter $2a^{WT}/\lambda$ | 0.12 | 0.76 |
| WEC diameter $2a^{WEC}/\lambda$ | 0.08 | 0.5 |
| Water depth $h/\lambda$ | 0.125 | 0.8 |
| Wave steepness $H/\lambda$ | 0.008 | 0.05 |

indicate that tested waves are in the range of linear and second-order Stokes waves.

### 3.2. Numerical model

The experimental investigation is supported by a numerical analysis based on the boundary element solver WAMIT [42]. The wind turbine and the WEC are represented using a higher-order method (ILOWHI = 1) that resulted in a total number of 1920 panels for two bodies (refer to Fig. 3). The excitation forces (Froude–Krylov and scattering components) are evaluated from the Haskind relations.

For basic geometries such as cylinders, analytical models are also available to calculate hydrodynamic forces. Thus, for the fixed-bottom cylinder that represents the monopile, an explicit mathematical expression was derived by MacCamy and Fuchs [43] for the total horizontal force:

$$\hat{F}^{WT}_{exc,x} = \frac{4\rho g a^{WT} A h}{k a^{WT} H_1'(k a^{WT})} \frac{\tanh kh}{kh}, \tag{5}$$

where $\rho$ is the water density, $g$ is the gravitational acceleration, $a^{WT}$ is the cylinder radius (monopile in our case), $A = H/2$ is the wave amplitude, $h$ is the water depth, $k = 2\pi/\lambda$ is the wave number, $H_1$ is the Henkel function of the first kind. For the isolated floating cylinder that represents the wave energy converter, the semi-analytical models were derived in [44,45].

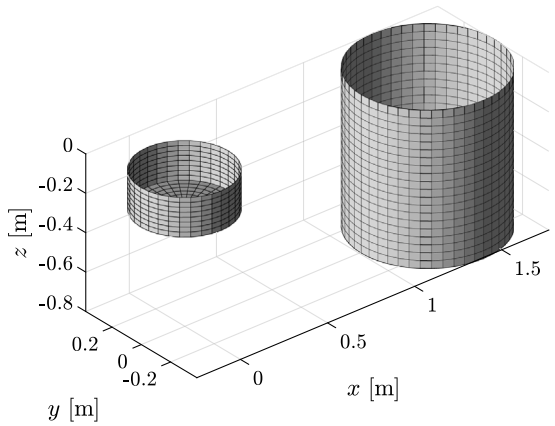


**Fig. 3.** Meshes of wind turbine substructure and WEC used in WAMIT to calculate hydrodynamic parameters.

### 3.3. Comparison between numerical and experimental data

Before conducting the primary set of experiments related to the effect of the WEC motion on the wind turbine substructure loading, the hydrodynamic parameters of the combined wind-wave system are first compared using sets of analytical (limited cases), numerical and experimental data. Firstly, the diffraction tests are carried out to investigate the wave loading on fixed bodies. These tests are conducted in three different configurations: (1) isolated wind turbine (without WEC) substructure, (2) isolated fixed WEC (without wind turbine), and (3) co-located wind turbine substructure and a fixed WEC. The wave amplitude across all diffraction tests is kept at 25 mm. Horizontal wave excitation forces acting on the wind turbine substructure in the absence and in the presence of the fixed WEC evaluated using the numerical solver WAMIT and experimentally are compared in Fig. 4(a). The force values calculated using Eq. (5) are also added to Fig. 4(a) for reference (marked as *analytical*). The results demonstrate a perfect match between the analytical and numerical models of an isolated wind turbine. However, in comparison with the experimental data, the numerical solver overestimates the horizontal force (surge) acting on the wind turbine substructure by approximately 10%.

Both numerical and experimental results demonstrate that diffraction effects created by the fixed WEC reduce the total loading on the wind turbine substructure in the range of wave periods between 1 and 1.5 s. Here, the wave period is defined as the time in seconds between successive rising-edge zero-crossings from the still water level and is measured with a resistive wave probe in-phase to the WEC. Where possible, hydrodynamic responses (including wave periods, forces, moments, etc.) are averaged across ten steady-state wave periods, consistent with International Towing Tank Conference guidelines [46]. The maximum reduction in the horizontal force of 15% is achieved at $T = 1.22$ s that corresponds to $ka^{WT} \approx 1$ (or $ka^{WEC} \approx 0.7$, or $kD \approx 4$).

The heave excitation forces acting on the fixed WEC with and without a wind turbine substructure are compared in Fig. 4(b). The heave excitation force experienced by the isolated WEC is also calculated using a semi-analytical model [45] and added to the plot for reference. In contrast to the case of a bottom-mounted wind turbine, the forces acting on the WEC calculated numerically and experimentally are in good agreement with each other. The force curve in the presence of the wind turbine substructure is found to oscillate around the curve of the isolated WEC demonstrating how interaction between two bodies can be either strengthened or weakened depending on the wave period.

Following the diffraction analysis, the WEC radiation tests are carried out to study the effect of the WEC heave motion on the wind turbine's horizontal force. During these tests, there are no incident

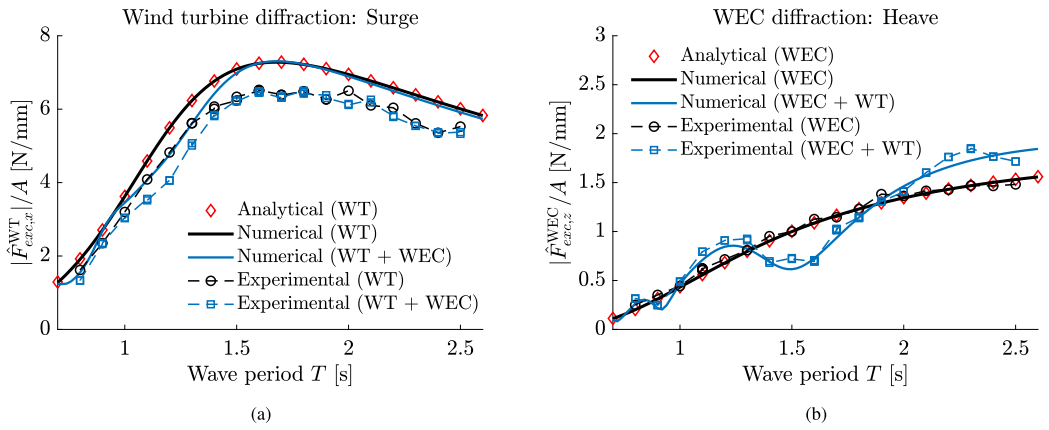


**Fig. 4.** Wave diffraction forces acting (a) on the wind turbine substructure in surge, and (b) on the WEC in heave. A comparison is made between forces obtained through the physical experiments (lines with markers) and using the numerical model (solid lines). The wave amplitude is set to 25 mm.

**Table 3**
Experimental test matrix for the motion optimisation study.

| Wave period | Number of phases | Number of amplitudes for optimal phase |
|---|---|---|
| 1.1 s | 8 | – |
| 1.3 s | 25 | 8 |
| 1.5 s | 7 | – |
| 1.7 s | 17 | 8 |
| 1.9 s | 6 | – |
| 2.1 s | 8 | 8 |

waves and loads acting on the wind turbine are measured when the WEC is forced to oscillate in heave with an amplitude of 25 mm. Using recorded time series of the wind turbine force $F^{WT}_{tot,x}(t)$ and WEC displacement $z^{WEC}(t)$, the first harmonic complex amplitudes of the corresponding signals ($\hat{F}^{WT}_{tot,x}$ and $\hat{z}^{WEC}$) are calculated for each frequency tested. Using Eq. (3) and keeping in mind that $\hat{F}^{WT}_{exc,x} = 0$ in this case, the added mass and damping coefficients are estimated using the following relationships:

$$A_{1,9} = \Re\mathfrak{e}\left\{\frac{\hat{F}^{WT}_{tot,x}}{\omega^2 \hat{z}^{WEC}}\right\}, \quad B_{1,9} = -\Im\mathfrak{m}\left\{\frac{\hat{F}^{WT}_{tot,x}}{\omega \hat{z}^{WEC}}\right\}. \tag{6}$$

The hydrodynamic coefficients estimated experimentally are compared in Fig. 5 with those calculated using the numerical model. A good agreement is observed between experimental and numerical results with a maximum deviation of 10%.

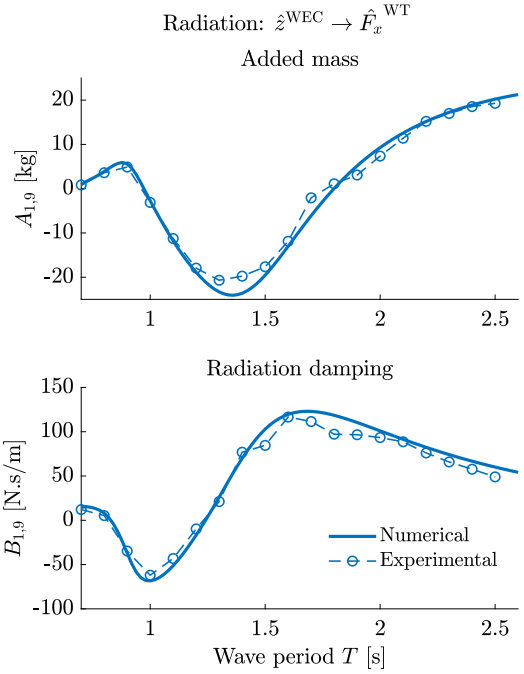


**Fig. 5.** The added mass and radiation-damping coefficients that define the hydrodynamic coupling between the WEC heave motion ($z^{WEC}$) and the wind turbine horizontal force ($F_x^{WT}$).

## 4. Motion optimisation of the WEC

As demonstrated in Section 2, the WEC motion (phase and amplitude) will affect the loading on the wind turbine substructure. A set of experiments is conducted to validate this theory focusing on the wind turbine horizontal force only. The wave amplitude is set to 25 mm, and six wave periods are tested between 1.1 s and 2.1 s with a step of 0.2 s. Firstly, the WEC motion amplitude is set to 25 mm, and its phase is varied relative to the phase of the incoming wave in order to find an optimal value that leads to the lowest total horizontal force acting on the wind turbine substructure. Then, setting the WEC phase to the optimal value, the WEC motion amplitude is scaled from 25 mm using multiplication factors between 0.5 and 4 with a step of 0.5. So the maximum WEC amplitude tested is $4 \times 25$ mm = 100 mm. The test matrix of these experiments is shown in Table 3.

In order to vary the phase of the WEC motion relative to the wave elevation phase, the following procedure is followed. The wave probe is placed in line with the WEC centre perpendicular to the incoming wave front. Then, the WEC motion is adjusted such that the WEC oscillates in phase with the incident wave (phase difference is zero in this case). Then a time delay is introduced into the linear actuator so the WEC motion lags the wave elevation (see experimental data in Fig. 6). The presented phase difference is calculated based on the set time delay and the wave frequency. Using the wave elevation ($\eta$) at the WEC location as a reference, it is valid to assume that the wave elevation has a phase zero:

$$\eta^{WEC}(t) = A\cos(\omega t). \tag{7}$$

Then, the WEC motion amplitude $z_0$ and phase $\varphi^{WEC}$ are calculated using the following convention:

$$z^{WEC}(t) = z_0 \cos\Big(\omega(t - \Delta t)\Big) = z_0 \cos\left(\omega t - \varphi^{WEC}\right). \tag{8}$$

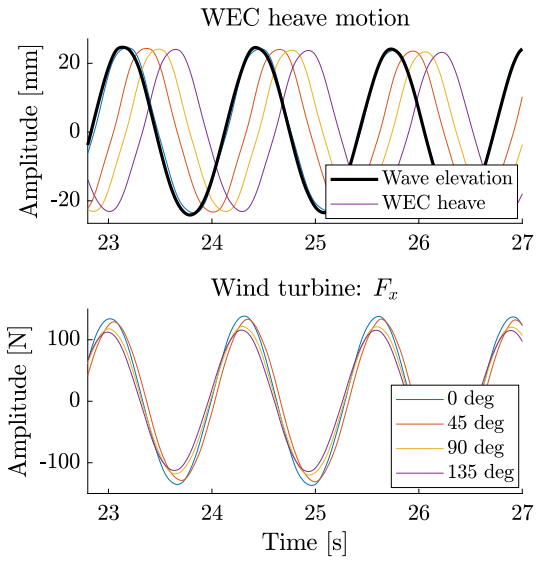


**Fig. 6.** Adjustment of the WEC motion phase relative to the wave elevation phase in a regular wave of $T = 1.3$ s during experiments.

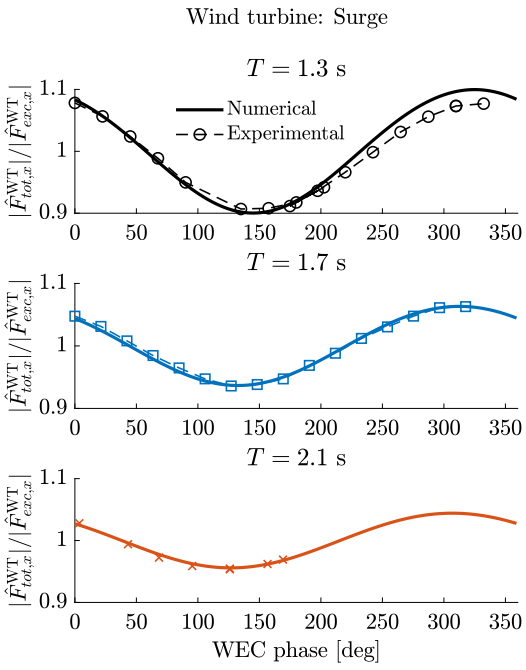


**Fig. 7.** Effect of the WEC motion phase on the wind turbine horizontal force in regular waves of $T = 1.3$, 1.7 and 2.1 s. Both the incident wave amplitude and the WEC heave amplitude are set to 25 mm.

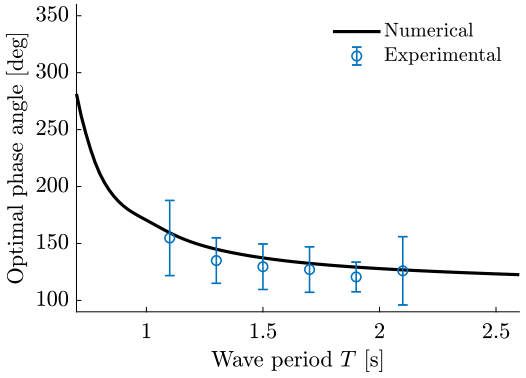


**Fig. 8.** Dependence of the optimal phase angle of the WEC motion to minimise load on the wind turbine as a function of wave period. Whiskers on the plot correspond to the step size of the experimental search for the optimal phase angle.

### 4.1. Phase sensitivity

The effect of the WEC motion phase on the wind turbine substructure horizontal loading is shown in Fig. 7 for three different wave periods $T = 1.3$, 1.5 and 2.1 s. In order to understand how WEC motion affects changes in the wind turbine force, the force amplitude is normalised to the force experienced by the wind turbine when the WEC is fixed (refer to Eq. (3)):

$$\frac{|\hat{F}^{WT}_{tot,x}|}{|\hat{F}^{WT}_{exc,x}|}. \tag{9}$$

The results demonstrate that despite differences between the numerical model and physical experiments, that have been shown in Fig. 4, both approaches demonstrate close agreement in this phase sensitivity study. By keeping the WEC motion amplitude at 25 mm, it is possible to reduce the horizontal force acting on the wind turbine substructure by up to 10%. Moreover, there are cases when the WEC motion can negatively affect the wind turbine by increasing the loading. Also, the optimal phase of the WEC motion that minimises the wind turbine horizontal force is different for different wave periods.

According to Eq. (3), it is possible to derive an expression for the optimal phase of the WEC motion as a function of the wave period following the phase definition from Eqs. (2) and (8):

$$\varphi^{WEC}_{opt} = -\varphi^{F^{WT}_{exc,x}} + \operatorname{atan}\left(\frac{B_{1,9}}{-\omega A_{1,9}}\right). \tag{10}$$

A comparison of the numerically predicted optimal phase and the one identified experimentally across a range of wave periods is presented in Fig. 8. Error bars on the plot correspond to the step size of the experimental search for the optimal phase angle. A close match is achieved for all wave periods tested.

### 4.2. Amplitude sensitivity

Once the optimal phase of the WEC motion is identified, it is possible to further reduce the loading on the wind turbine by increasing the WEC motion amplitude as per Eq. (3). This effect is shown in Fig. 9 for three wave periods of $T = 1.3$, 1.7 and 2.1 s. The incident wave amplitude is set constant to 25 mm across all wave periods tested. The WEC heave amplitude is varied between 12.5 mm and 100 mm. As predicted by the linear wave theory, experimental results demonstrate a linear dependence of the wind turbine force and the WEC heave amplitude. The greatest reduction in the force of up to 40% is achieved at the wave period of 1.3 s.

In order to demonstrate the overall effect that the presence of the WEC (either fixed or oscillating) have on the wind turbine horizontal force, the results from Figs. 4(a), 7, 8 and 9 are combined from the experimental and numerical investigations on Figs. 10(a) and 10(b) respectively. This comparison clearly demonstrates that some reduction in the wind turbine loading is due to the diffraction effects from the fixed WEC, while the force reduction is more significant when the WEC is oscillating.

### 4.3. Absorbed power

It is possible to estimate how much energy has been absorbed by the WEC in order to achieve the reduction in loading reported in Figs. 10(a) and 10(b). This is shown in Fig. 11 based on the numerical and experimental data. It should be noted that some discrepancy between

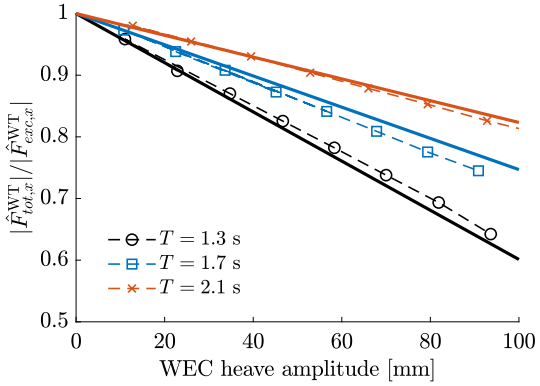


**Fig. 9.** Effect of the WEC motion amplitude on the wind turbine horizontal force in regular waves of $T = 1.3$, 1.7 and 2.1 s. The incident wave amplitude is set to 25 mm, and the WEC phase angle is set to the optimal value identified experimentally according to Fig. 8.

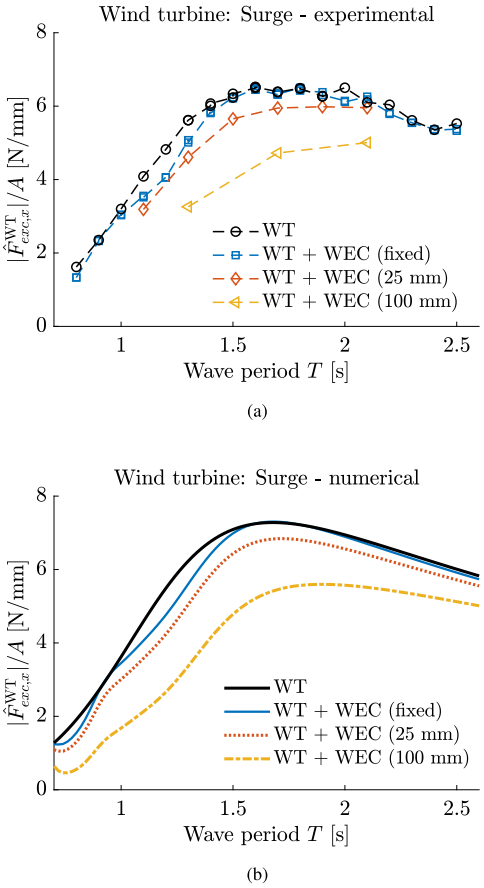


**Fig. 10.** Effect of the WEC (fixed or oscillating) on the wind turbine horizontal force evaluated (a) experimentally, and (b) numerically. The wave amplitude is 25 mm. In the legend, values in brackets correspond to the WEC motion amplitude, while the WEC phase is set to the optimal value according to Fig. 8.

power values calculated from numerical and physical experiments is mainly due to the difference in the WEC optimal phase angle, which was only measured at discrete 30 deg intervals (refer to Fig. 8). Fig. 11 demonstrates that for this particular geometry of the problem, a simultaneous WEC power absorption and wind turbine load reduction is only possible for waves longer than 1.5 s, which is shown as a positive power output in Fig. 11. However, this is not achievable in waves shorter than 1.5 s, where the WEC should be actuated by drawing power from the

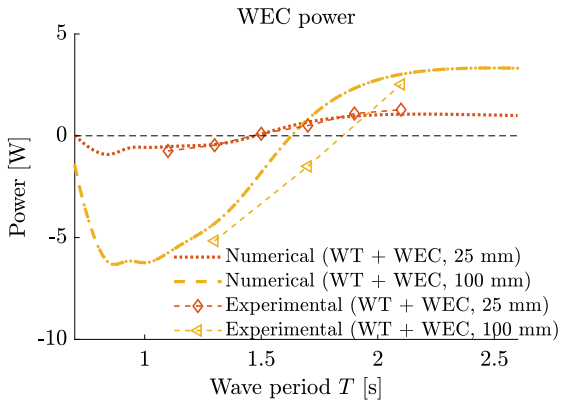


**Fig. 11.** The power absorbed by the WEC in order to achieve the reduction in wind turbine horizontal force reported in Fig. 10(b). Positive values indicate power generated by the WEC, negative values indicated power consumed by the WEC.

grid or storage in order to effectively reduce the horizontal force on the wind turbine substructure.

## 5. Power absorption vs. load reduction

During conducted experiments, the WEC has been forced to oscillate with the required amplitude and phase regardless of the force and power input. In the real wind-wave system, the WEC is excited by incident waves and its motion is directly dependent on the settings of the PTO machinery and the control algorithm. The dynamics of the PTO unit is usually approximated by the spring–damper system, and there are two main control strategies widely used in wave energy, namely active and passive controls. If active control is applied, the PTO should act either as a generator or as a motor, depending on the part of the WEC motion cycle. In the case of passive control, the PTO always operates in generator mode. With these two control options in mind, the trade-off between WEC power absorption and wind turbine load reduction is investigated in this section using numerical analysis.

In the combined wind-wave system, the motion of the WEC, connected to the PTO machinery, under the regular wave loading can be described by the following equation (assuming the linearity of the problem):

$$\left[-\omega^2(m + A_{9,9}) + i\omega(B_{9,9} + B_{pto}) + (K_{hs} + K_{pto})\right] \hat{z}^{WEC} = \hat{F}^{WEC}_{exc,z}. \tag{11}$$

where $m$ is the WEC mass, $A_{9,9}$ and $B_{9,9}$ are the WEC's added mass and radiation damping coefficients in heave, $K_{pto}$ and $B_{pto}$ are linear power take-off stiffness and damping coefficients, $K_{hs}$ is the hydrostatic stiffness. Once the WEC motion is known, the average power absorbed by the WEC in a regular wave can be calculated as:

$$\overline{P} = \frac{1}{2} B_{pto} \omega^2 |\hat{z}^{WEC}|^2. \tag{12}$$

Let us consider two objective functions that can be optimised by tuning the PTO parameters $K_{pto}$ and $B_{pto}$, taking into account the limited stroke of the WEC:

1. maximise WEC power output (Eq. (12)):

$$\arg\max_{K_{pto}, B_{pto}} \overline{P}, \text{ subject to: } |\hat{z}^{WEC}| \leq 0.2 \text{ m}. \tag{13}$$

2. minimise the wind turbine horizontal force (Eq. (3)):

$$\arg\min_{K_{pto}, B_{pto}} \hat{F}^{WT}_{tot,x}, \text{ subject to: } |\hat{z}^{WEC}| \leq 0.2 \text{ m}. \tag{14}$$

Moreover, each objective function is investigated using two different control scenarios: (1) with active control of the WEC where both $K_{pto}$ and $B_{pto}$ are kept as optimisation parameters that can take both

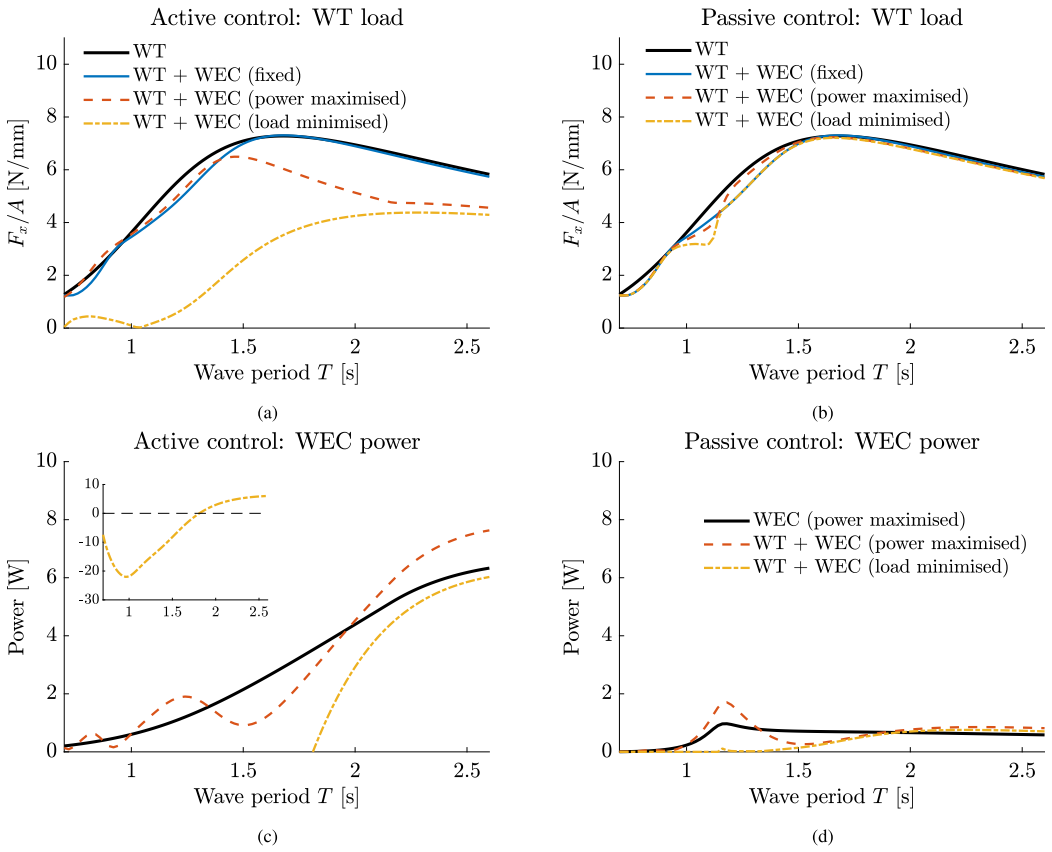


**Fig. 12.** Effect of WEC motion on wind turbine horizontal force and WEC power output depending on the objective function: either power maximisation or load minimisation. The results are obtained using the numerical model for the active and passive control approaches. The wave amplitude is 25 mm.

negative and positive values; and (2) with passive control of the WEC where $K_{pto} = 0$ and $B_{pto} > 0$. Fig. 12 demonstrates the optimisation results that can be summarised as follows (the corresponding values of optimised PTO parameters are shown in Appendix). If active control is used, it is possible to:

- significantly reduce the wave loading on the wind turbine (up to 100%) in short waves ($T < 1$ s) but with an energy input to the WEC;
- slightly increase the horizontal force acting on the wind turbine substructure when power is maximised in short waves;
- simultaneously achieve power absorption and load reduction (up to 20%) in long waves ($T > 2$ s);
- absorb four times more power than using passive control in longer waves (Figs. 12(b) and 12(d)).

A passively controlled WEC has a very limited effect on wind turbine loading and power production. As shown in Fig. 12(b) and discussed in Section 3.3, having a fixed WEC in front of the wind turbine substructure reduces the wave load by a maximum of 15% in a range of periods from 1 to 1.5 s. A further reduction in wave load can be achieved by passively controlling the motion of a WEC, but this effect is limited to a range of wave periods close to the natural period of this WEC (1.15 s). Taking into account that the WEC equipped with passive control does not produce any power in the range of periods below 1.5 s (refer to Fig. 12(d)), it may be concluded, that the fixed WEC would be more beneficial to the wind-wave system than the WEC with a passive control system.

However, it should be noted that these results are valid only for the specific geometry of the problem under consideration (radii of a WEC and a wind turbine substructure, as well as the distance between structures). To achieve simultaneous power production and load reduction for a particular wave climate, it is required to optimise the entire configuration taking into account the feasible control solution (either active or passive control approach).

## 6. Discussion

The following discussion outlines some of the limitations of this study and provides recommendations for future work.

1. The geometry and spatial arrangement of the wind-wave system in this study is limited to one configuration. It is likely that different geometrical configurations may produce different results. Future work should investigate alternative configurations and arrays of WECs.
2. The interactions between the co-located wind-wave system are tested in small-amplitude regular waves to draw clear conclusions about the effect of the WEC's heave motion on wind turbine wave loading. However, extreme wave loading generated by very large irregular waves is not presented in this study. Evaluating the survivability characteristics of the WEC and wind turbine structures in highly nonlinear waves is an important next step as wave slamming, wave run-up, and overtopping (i.e., greenwater) are critical factors for survivability. Future works recommend investigating the interaction between the WEC's motions and wind turbine wave loading when exposed to highly nonlinear focused wave groups.
3. The WEC's motion is limited to heave in this study. In a more realistic scenario, the WEC will likely surge forward and aft (depending on the mooring system). The effect of coupled heave and surge motions should be also investigated.
4. The motion of the WEC in this study was kinematically controlled by a linear actuator, which made it possible to eliminate the uncertainties associated with the implementation of active control. Future work should include real-time active control of the WEC in physical experiments to provide more accurate estimates of the power generated by the WEC.

## 7. Conclusion

In this work, a combined wind-wave system is investigated to understand the effect of WEC motion on wind turbine loads using intensive physical experiments. The results demonstrate that the horizontal force acting on the wind turbine substructure can be decreased by up to 40% subject to the WEC phase, amplitude and wave frequency. Also, there is a linear relationship between the WEC motion amplitude and the wind turbine horizontal force. In longer wave periods, the WEC can generate both power while also reducing the load on the wind turbine substructure. However, in shorter waves, these two goals contradict each other, and the WEC should be actuated and draw power from the grid in order to minimise the wind turbine loads. Also, a comparison is made between active and passive WEC control strategies, and it is found that only active control is suitable for this goal. A passively controlled WEC has a very limited effect on wave-induced wind turbine forces.

## CRediT authorship contribution statement

**Eric Gubesch:** Conceptualization, Methodology, Validation, Formal analysis, Investigation, Writing – original draft. **Nataliia Y. Sergienko:** Conceptualization, Methodology, Software, Validation, Formal analysis, Writing – original draft, Visualization. **Jean-Roch Nader:** Methodology, Formal analysis, Writing – review & editing, Supervision. **Boyin Ding:** Conceptualization, Writing – review & editing, Supervision, Project administration. **Benjamin Cazzolato:** Methodology, Formal analysis, Writing – review & editing, Supervision, Funding acquisition. **Irene Penesis:** Writing – review & editing, Supervision, Project administration. **Ye Li:** Methodology, Writing – review & editing, Supervision, Funding acquisition.

## Declaration of competing interest

The authors declare that they have no known competing financial interests or personal relationships that could have appeared to influence the work reported in this paper.

## Acknowledgements

The authors acknowledge the funding support of Australia-China Science and Research fund, Australian Department of Industry, Innovation and Science (ACSRF66211), and the Ministry of Science and Technology of China (2017YFE0132000). The technical support provided during the experiments by the following individuals is acknowledged: Assoc. Professor Gregor MacFarlane, Dr. Nick Johnson, Liam Honeychurch, Kye Curwen, Toby Davis, Nagi Abdussamie, Jack Crawford and Shelby Hewins, Australian Maritime College, University of Tasmania. Author Penesis' time was supported under the Blue Economy Cooperative Research Centre, established and supported under the Australian Government's Cooperative Research Centres Program (grant number CRC-20180101).

## Appendix. Optimised power take-off parameters

Fig. A.13 demonstrates values of the optimised power take-off parameters identified in Section 5 for two objective functions: maximisation of the WEC power output and minimisation of the wave loading acting on the wind turbine substructure using active and passive control laws. When active control is used either to maximise WEC power or minimise the wave loading, the negative stiffness is required to be provided for longer wave periods in order to adjust the natural frequency of the WEC. This can be achieved by using bistable mechanisms [47]. Also, to reduce wave loads on the wind turbine substructure, the PTO

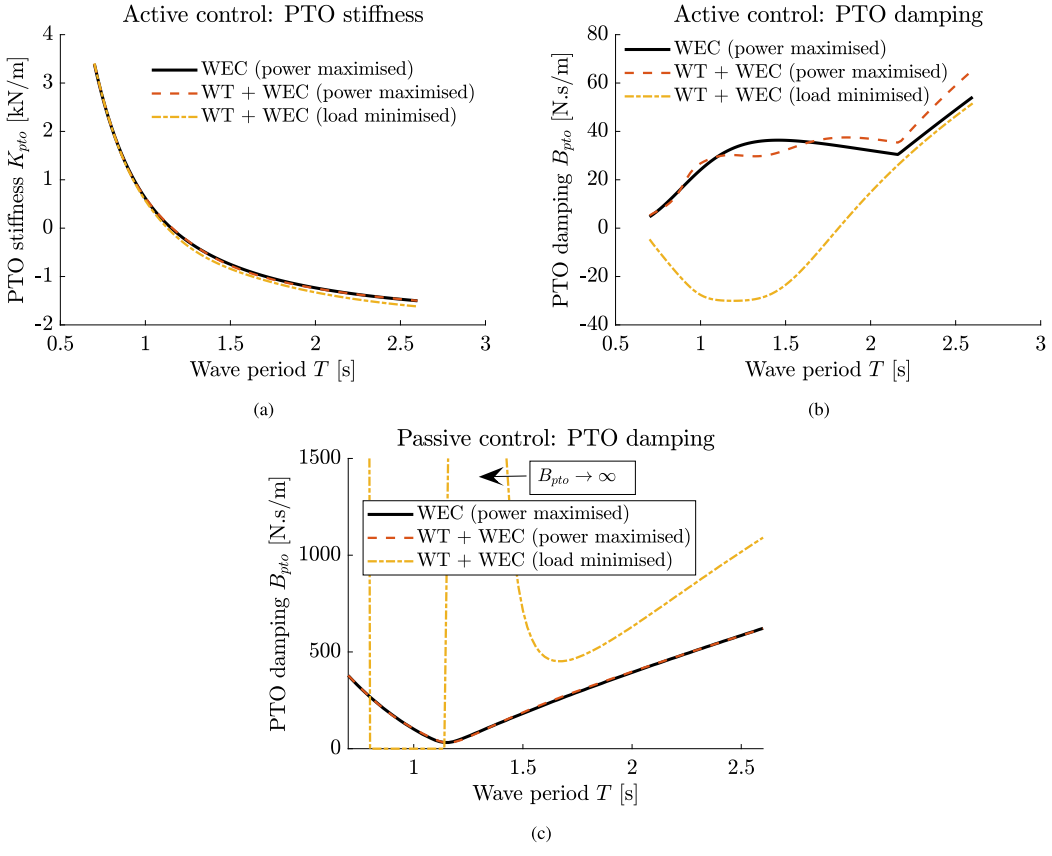


**Fig. A.13.** Values of the optimised power take-off parameters used to produce Fig. 12.

damping should take negative values over a range of wave periods below 1.8 s which corresponds to the situation of supplying power to the WEC instead of generating useful electricity (refer to Fig. 12(c)).

Interestingly, when passive WEC control is used for load reduction, there is a range of wave periods (1.1 s $< T <$ 1.4 s) where it is more beneficial to keep the WEC fixed which is evident by very large values of the PTO damping, $B_{pto} \rightarrow \infty$. In this case, the major changes in the wavefield are caused by the WEC diffraction and not WEC radiation, a similar conclusion is also reported in [48].

## References


[1] IRENA, Renewable capacity statistics 2021, International Renewable Energy Agency (IRENA), Report, 2021, Abu Dhabi.

[2] IRENA, Offshore Renewables: An Action Agenda for Deployment, Report, International Renewable Energy Agency, Abu Dhabi, United Arab Emirates, 2021.

[3] IEA, World Energy Outlook 2021, Technical Report, International Energy Agency, 2021.

[4] R. Mayon, D. Ning, B. Ding, N.Y. Sergiienko, Wave energy converter systems – status and perspectives, in: Modelling and Optimization of Wave Energy Converters, CRC Press, 2022, pp. 3–58.

[5] W. Musial, P. Spitsen, P. Duffy, P. Beiter, M. Marquis, R. Hammond, M. Shields, Offshore Wind Market Report: 2022 Edition, Technical Report, National Renewable Energy Lab (NREL), Golden, CO (United States), 2022.

[6] X. Wu, Y. Hu, Y. Li, J. Yang, L. Duan, T. Wang, T. Adcock, Z. Jiang, Z. Gao, Z. Lin, A. Borthwick, S. Liao, Foundations of offshore wind turbines: A review, Renew. Sustain. Energy Rev. 104 (2019) 379–393.

[7] D. Kallehave, B.W. Byrne, C. LeBlanc Thilsted, K.K. Mikkelsen, Optimization of monopiles for offshore wind turbines, Phil. Trans. R. Soc. A 373 (2035) (2015) 20140100.

[8] X. Chen, Z. Jiang, Q. Li, Y. Li, N. Ren, Extended environmental contour methods for long-term extreme response analysis of offshore wind turbines, J. Offshore Mech. Arct. Eng. 142 (2020) 052003.

[9] Z. Gao, X. Feng, Z. Zhang, Z. Liu, X. Gao, L. Zhang, S. Li, Y. Li, A brief discussion on offshore wind turbine hydrodynamics problem, J. Hydrodyn. 34 (2013) 15–30.

[10] Z. Jiang, Z. Gao, Z. Ren, Y. Li, L. Duan, A parametric study on the final blade installation process for monopile wind turbines under rough environmental conditions, Eng. Struct. 172 (2018) 1042–1056.

[11] E. Gubesch, C. Chin, N. Abdussamie, I. Penesis, The hydrodynamic performance of an integrated semi-submersible platform with wave energy converters: A concept for multi-use platforms, in: Australasian Coasts & Ports Conference 2019, 2019, pp. 1–7.

[12] L. da Silva, N. Sergiienko, B. Cazzolato, B. Ding, Dynamics of hybrid offshore renewable energy platforms: Heaving point absorbers connected to a semi-submersible floating offshore wind turbine, Renew. Energy 199 (2022) 1424–1439.

[13] L.S. da Silva, B. Ding, B. Guo, N.Y. Sergiienko, Wave energy converter modelling, control, and power take-off design, in: Modelling and Optimization of Wave Energy Converters, CRC Press, 2022, pp. 97–128.

[14] F. Meng, N. Sergiienko, B. Ding, B. Zhou, L.S.P. Da Silva, B. Cazzolato, Y. Li, Co-located offshore wind–wave energy systems: Can motion suppression and reliable power generation be achieved simultaneously? Appl. Energy 331 (2023) 120373.

[15] C. Pérez-Collazo, D. Greaves, G. Iglesias, A review of combined wave and offshore wind energy, Renew. Sustain. Energy Rev. 42 (2015) 141–153.

[16] S. Astariz, G. Iglesias, Enhancing wave energy competitiveness through co-located wind and wave energy farms. a review on the shadow effect, Energies 8 (7) (2015) 7344–7366.

[17] O.W.C. Ltd., Opportunities for sharing infrastructure, services and supply chain, Technical Report, Wave Energy Scoltland, 2023.

[18] C. Perez-Collazo, D. Greaves, G. Iglesias, A novel hybrid wind-wave energy converter for jacket-frame substructures, Energies 11 (3) (2018) 637.

[19] C. Perez-Collazo, R. Pemberton, D. Greaves, G. Iglesias, Monopile-mounted wave energy converter for a hybrid wind-wave system, Energy Convers. Manage. 199 (2019) 111971.

[20] N. Ren, Z. Ma, T. Fan, G. Zhai, J. Ou, Experimental and numerical study of hydrodynamic responses of a new combined monopile wind turbine and a heave-type wave energy converter under typical operational conditions, Ocean Eng. 159 (2018) 1–8.

[21] C. Jiang, R. Gao, F. Cao, H. Shi, Structural energy transfer to the jacket foundation of an offshore wind-wave coupling device based on absolute transmissibility function, Appl. Ocean Res. 137 (2023) 103605.

[22] B. Fenu, M. Bonfanti, A. Bardazzi, C. Pilloton, A. Lucarelli, G. Mattiazzo, Experimental investigation of a multi-OWC wind turbine floating platform, Ocean Eng. 281 (2023) 114619.

[23] B. Zhou, J. Hu, Y. Wang, P. Jin, F. Jing, D. Ning, Coupled dynamic and power generation characteristics of a hybrid system consisting of a semi-submersible wind turbine and an array of heaving wave energy converters, Renew. Energy (2023).

[24] Floating Power Plant, Floating Power Plant – Invest in the future of energy, 2023, URL https://www.floatingpowerplant.com/, Retrieved on 17 August 2023.

[25] A. Yde, M.M. Pedersen, S.B. Bellew, A. Køhler, R.S. Clausen, A.W. Nielsen, Experimental and theoretical analysis of a combined floating wave and wind energy conversion platform, 2014.

[26] A. Yde, T.J. Larsen, A.M. Hansen, M. Fernandez, S. Bellew, F.P. Plant, Comparison of simulations and offshore measurement data of a combined floating wind and wave energy demonstration platform, J. Ocean. Wind Energy 2 (2015) 129–137.

[27] S. Astariz, G. Iglesias, Selecting optimum locations for co-located wave and wind energy farms. part I: The co-location feasibility index, Energy Convers. Manage. 122 (2016) 589–598.

[28] S. Astariz, G. Iglesias, Selecting optimum locations for co-located wave and wind energy farms. part II: A case study, Energy Convers. Manage. 122 (2016) 599–608.

[29] C.E. Clark, A. Miller, B. DuPont, An analytical cost model for co-located floating wind-wave energy arrays, Renew. Energy 132 (2019) 885–897.

[30] L. Castro-Santos, E. Martins, C.G. Soares, Economic comparison of technological alternatives to harness offshore wind and wave energies, Energy 140 (2017) 1121–1130.

[31] H.D.P. Gonzalez, F.D. Bianchi, J.L. Dominguez-Garcia, O. Gomis-Bellmunt, Co-located wind-wave farms: Optimal control and grid integration, Energy 272 (2023) 127176.

[32] S. Astariz, C. Perez-Collazo, J. Abanades, G. Iglesias, Towards the optimal design of a co-located wind-wave farm, Energy 84 (2015) 15–24.

[33] S. Astariz, G. Iglesias, Accessibility for operation and maintenance tasks in co-located wind and wave energy farms with non-uniformly distributed arrays, Energy Convers. Manage. 106 (2015) 1219–1229.

[34] C.E. Clark, J. Velarde, J. Sønderkær Nielsen, Fatigue load reductions in offshore wind turbine monopile foundations in co-located wind-wave arrays, in: International Conference on Offshore Mechanics and Arctic Engineering, vol. 51975, American Society of Mechanical Engineers, 2018, V001T01A037.

[35] E. Gubesch, J.-R. Nader, B. Ding, B. Cazzolato, Y. Li, N. Sergiienko, I. Penesis, Experimental hydrodynamic investigation of a co-located wind turbine and wave energy converter, in: Proceedings of the ASME 2023 42nd International Conference on Offshore Mechanics and Arctic Engineering (OMAE2023), American Society of Mechanical Engineers, Melbourne, Australia, 2023, pp. OMAE2023–105348.

[36] J.-R. Nader, A. Fleming, G. Macfarlane, I. Penesis, R. Manasseh, Novel experimental modelling of the hydrodynamic interactions of arrays of wave energy converters, Int. J. Mar. Energy 20 (2017) 109–124.

[37] J. Falnes, P. McIver, Surface wave interactions with systems of oscillating bodies and pressure distributions, Appl. Ocean Res. 7 (4) (1985) 225–234.

[38] J. Falnes, A. Kurniawan, Ocean Waves and Oscillating Systems: Linear Interactions Including Wave-Energy Extraction, vol. 8, Cambridge University Press, 2020.

[39] E. Gaertner, J. Rinker, L. Sethuraman, F. Zahle, B. Anderson, G. Barter, N. Abbas, F. Meng, P. Bortolotti, W. Skrzypinski, et al., Definition of the IEA 15-Megawatt offshore reference wind turbine, Technical Report, National Renewable Energy Lab. (NREL), Golden, CO (United States), 2020.

[40] N. Sergiienko, L. da Silva, E. Bachynski-Polić, B. Cazzolato, Review of scaling laws applied to floating offshore wind turbines, Renew. Sustain. Energy Rev. 162 (2022) 112477.

[41] G. Mogridge, W. Jamieson, Wave Loads on Large Circular Cylinders: A Design Method (Forces des Houles sur des Cylindres Circulaires: Methode de Calcul)., Technical Report, National Research Council of Canada Ottawa (Ontario) Hydraulics Lab, 1976.

[42] C.-H. Lee, WAMIT Theory Manual, Massachusetts Institute of Technology, 1995.

[43] R. MacCamy, R.A. Fuchs, Wave Forces on Piles: A Diffraction Theory, (69) US Beach Erosion Board, 1954.

[44] R.W. Yeung, Added mass and damping of a vertical cylinder in finite-depth waters, Appl. Ocean Res. 3 (3) (1981) 119–133.

[45] S.-c. Jiang, Y. Gou, B. Teng, D.-z. Ning, Analytical solution of a wave diffraction problem on a submerged cylinder, J. Eng. Mech. 140 (1) (2014) 225–232.

[46] ITTC, Analysis procedure for model tests in regular waves, in: ITTC Quality System Manual Recommended Procedure and Guidelines 7.5-02-07-03.2 Revision 2. International Towing Tank Conference, 2017, pp. 1–5.

[47] B.W. Schubert, N.Y. Sergiienko, B.S. Cazzolato, W.S. Robertson, M.H. Ghayesh, The true potential of nonlinear stiffness for point absorbing wave energy converters, Ocean Eng. 245 (2022) 110342.

[48] S. Hewins, J.-R. Nader, E. Gubesch, N. Sergiienko, Positive interaction of hydrodynamic motions of an offshore wind turbine with co-located WEC, in: Proceedings of the ASME 2023 42nd International Conference on Offshore Mechanics and Arctic Engineering (OMAE2023), American Society of Mechanical Engineers, Melbourne, Australia, 2023, pp. OMAE2023–105352.